Influence of Molecular Shape on Solid-State Packing in Disordered PC61BM and PC71BM Fullerenes

ARTICLE *in* JOURNAL OF PHYSICAL CHEMISTRY LETTERS · OCTOBER 2014

Impact Factor: 7.46 · DOI: 10.1021/jz501559q

5 AUTHORS, INCLUDING:

Saadullah G. Aziz
King Abdulaziz University
62 PUBLICATIONS **162** CITATIONS
SEE PROFILE

Chad Risko
University of Kentucky
93 PUBLICATIONS **2,564** CITATIONS
SEE PROFILE

THE JOURNAL OF PHYSICAL CHEMISTRY Letters

Letter

pubs.acs.org/JPCL

Influence of Molecular Shape on Solid-State Packing in Disordered $PC_{61}BM$ and $PC_{71}BM$ Fullerenes

Monika Williams,[†,#] Naga Rajesh Tummala,[†] Saadullah G. Aziz,[‡] Chad Risko,*[,†,§] and Jean-Luc Brédas*[,†,‡,⊥]

[†]School of Chemistry and Biochemistry & Center for Organic Photonics and Electronics, Georgia Institute of Technology, Atlanta, Georgia 30332, United States

[‡]Department of Chemistry, King Abdulaziz University, Jeddah 21589, Kingdom of Saudi Arabia

Supporting Information

ABSTRACT: Molecular and polymer packings in pure and mixed domains and at interfacial regions play an important role in the photoconversion processes occurring within bulk heterojunction organic solar cells (OSCs). Here, molecular dynamics simulations are used to investigate molecular packing in disordered (amorphous) phenyl-C_{70}–butyric acid–methyl ester ($PC_{71}BM$) and its C_{60} analogue ($PC_{61}BM$), the two most widely used molecular-based electron-accepting materials in OSCs. The more ellipsoidal character of $PC_{71}BM$ leads to different molecular packings and phase transitions when compared to the more spherical $PC_{61}BM$. Though electronic structure calculations indicate that the average intermolecular electronic couplings are comparable for the two systems, the electronic couplings as a function of orientation reveal important variations. Overall, this work highlights a series of intrinsic differences between $PC_{71}BM$ and $PC_{61}BM$ that should be considered for a detailed interpretation and modeling of the photoconversion process in OSCs where these materials are used.

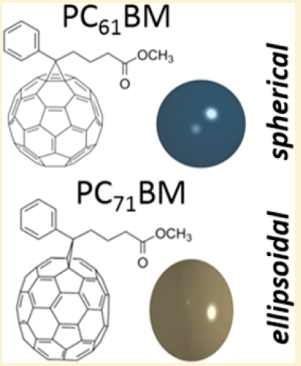

SECTION: Energy Conversion and Storage; Energy and Charge Transport

Organic solar cells (OSCs),[1−5] in which the active layer is a multicomponent thin film consisting of an electron-poor, acceptor (electron-transport) constituent and an electron-rich, donor (hole-transport) constituent, have potential to become a high-impact solar energy harvesting technology. While the main processes that underlie photocurrent generation are generally recognized,[6−12] there lacks a comprehensive understanding of the relationships between the electron- and energy-transfer processes and molecular packings in the bulk-like and mixed/interfacial regions of the film. Hence, a priori design principles for new generations of molecular and polymer constituents remain narrow.

Irrespective of this limited understanding, considerable advances in OSC power conversion efficiencies (PCEs) continue to be made due to improved materials and optimized processing protocols. Single-junction OSCs making use of the bulk heterojunction (BHJ) thin film architecture have broken 9% PCE for polymer (donor)–fullerene (acceptor) blends and 8% PCE for molecule (donor)–fullerene (acceptor) blends, while tandem (multiple junction) solar cells are now beyond 10% PCE.[13,14] A common feature of all high-performing BHJ solar cells is the use of substituted fullerenes (typically based on C_{60} and C_{70}) as the acceptor component. Of the substituted fullerenes, $PC_{61}BM$ and $PC_{71}BM$ ([6,6]-phenyl-$C_{61/71}$–butyric acid–methyl ester) are the most widely used and successful analogues (Figure 1).[15,16] The combination of appropriate electron affinity (with respect to the ionization potential and electron affinity of the donor component and Fermi energy of electron-collecting electrodes), material miscibility, and three-dimensional charge carrier transport properties are considered to be key aspects to the success of these systems.[17] Though much effort has been undertaken to design new acceptor systems to improve light absorption and reduce materials' costs, the best devices with alternative fullerene acceptors have PCEs generally in the range of 3–4%,[18,19] with recent works improving the efficiency to 6% with a perylene bisamide acceptor;[20] also, the use of an energy-cascade trilayer architecture has resulted in 8.4% PCE.[21] The majority use of fullerenes emphasizes the need to characterize at the molecular level the intrinsic properties that lead to the impact of the fullerene-based materials, with the goal of improving our understanding of the basic OSC photoconversion process and developing new materials' design protocols.

A key difference between $PC_{61}BM$ and $PC_{71}BM$ is the ellipsoidal shape of the latter as compared to the more spherical C_{60} analogue. The lower symmetry and more extended conjugation of C_{70} leads to a broader photoabsorption profile in the visible region of the electromagnetic spectrum, an important attribute that has brought the C_{70} analogue to the forefront of OSC research (despite its higher cost).[22] However, the ellipsoidal structure has also been ascribed to diminished solubility and leads to isomeric variations; $PC_{71}BM$ molecular

Received: July 24, 2014
Accepted: September 17, 2014
Published: September 17, 2014

   dx.doi.org/10.1021/jz501559q | J. Phys. Chem. Lett. 2014, 5, 3427−3433

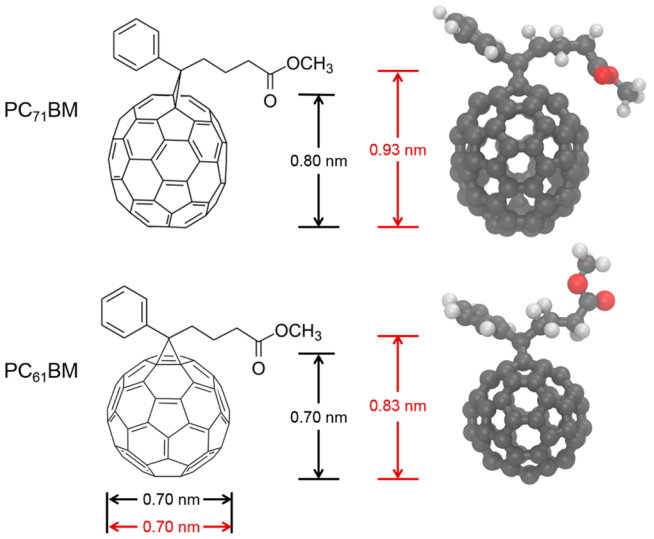

Figure 1. Molecular structures and shapes of $PC_{71}BM$ (top) and $PC_{61}BM$ (bottom). Axial distances in black are for the fullerene moiety only, while the distances in red also take into account the methano-bridge carbon, that is, the carbon atom connected to the fullerene cage. The denoted distances are between the carbon atom nuclei, without taking the van der Waals radii of the atoms into account. Representative ball and stick figures of $PC_{71}BM$ and $PC_{61}BM$ are shown at the far right.

materials are comprised of an 85:15 α/β isomeric blend, with the regioisomers arising from different attachment points of the phenyl–butyric acid–methyl ester moieties on the fullerene cage.[15,23] We note that the occurrence of fullerene isomers has been suggested to reduce the effectiveness of multiadduct fullerenes in OSCs.[24−26]

The differences in the fullerene shapes can lead to molecular packing dissimilarities. With an aspect ratio of 1.14, $PC_{71}BM$ (fullerene moiety only, Figure 1) is a prolate ellipsoid. Prolate ellipsoids[27] with aspect ratios of 1.15 have been shown to pack in high-density configurations denoted as random jammed packings, where jammed packings are defined as configurations wherein the degrees of freedom of the individual molecules go to zero. We note that by taking into account the methano-bridge carbon, both $PC_{71}BM$ (1.33) and $PC_{61}BM$ (1.19) can be considered as prolate ellipsoids. However, the limited volume occupied by the methano-bridge carbon, while also complicating analysis of the packing characteristics due to the introduced asymmetry of the ellipsoid, can be considered as a minor perturbation to the volumes arising from the fullerenes. As such, it is reasonable to consider that packing differences between these substituted fullerenes arise mainly from the differences in the sphere and ellipsoid volumes of C_{60} and C_{70}, respectively.

Here, we extend previous theoretical investigations on $PC_{61}BM$[28−30] to $PC_{71}BM$ to discern how the intrinsic structural differences of these molecular materials impact molecular packing and the resulting intermolecular electronic couplings in the solid state. Such an understanding will be useful because it is commonly assumed that $PC_{61}BM$ and $PC_{71}BM$, and even C_{60}, are essentially (structurally) interchangeable, particularly in models developed to delineate the intrinsic processes of exciton dissociation and charge recombination.[31,32] Molecular dynamics (MD) simulations are employed to investigate a number of materials-scale properties, including melting and order–disorder transitions as well as Hildebrand[33] and Hansen[34] solubility parameters, while electronic structure calculations are used to examine the resulting intermolecular electronic couplings. For the $PC_{71}BM$ simulations, both a pure α-isomer material and an 85:15 α/β regioisomer blend are considered. Full details of the computational methodology are provided in the Supporting Information (SI).

As a first step to detail how the ellipsoidal shape of $PC_{71}BM$ affects its intermolecular interactions and reflects on its materials-scale properties, we evaluate the cohesive energy densities and Hildebrand[33] and Hansen[34] solubility parameters (Table S1 in the SI). The Hildebrand solubility parameter for $PC_{71}BM$, 10.55 $(cal/cm^3)^{1/2}$, is only slightly smaller than that of $PC_{61}BM$, 10.65 $(cal/cm^3)^{1/2}$.[28] As expected, the dispersive term is the largest contributing factor in each system. The solubility parameters for the $PC_{71}BM$ α/β blend are statistically identical to those for the pure α-isomer; however, we note that in actual volumes larger than those considered in our simulations (e.g., in thin films), there might exist the possibility for phase separation among the isomers. Importantly, the good comparison with experimental evaluations of the solubility parameters provides confidence in the methodology chosen for the simulation procedures.

Thermodynamic phase transitions are evaluated through *NPT* (constant number of molecules *N*, pressure *P*, and temperature *T*) MD simulations (Figure 2). Following reported procedures and plotting density versus temperature,[35,36] we find reasonable agreement with experiment; the melting temperature of the (majority) α-isomer occurs at 695 K, while the experimental melting point is reported at 592 K.[37] We note that this overestimation in the computed transition

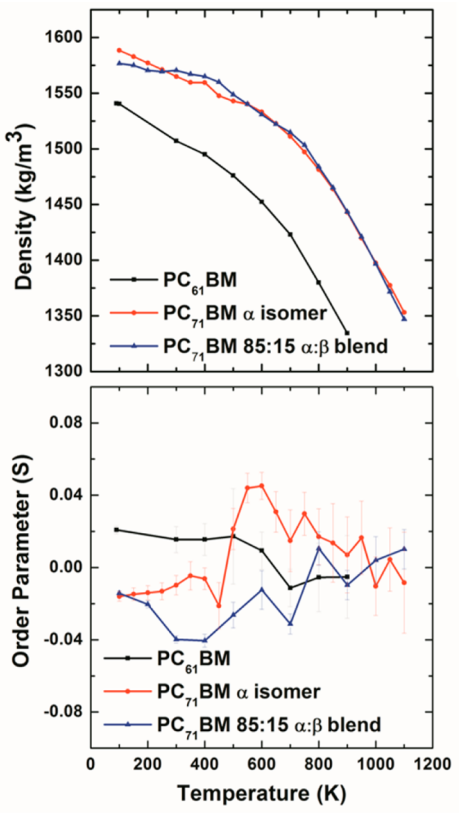

Figure 2. Density (top) and liquid-crystal order parameter (*S*) (bottom) as a function of temperature for amorphous $PC_{61}BM$ and for the pure α-phase and isomeric mixtures of amorphous $PC_{71}BM$.

dx.doi.org/10.1021/jz501559q | J. Phys. Chem. Lett. 2014, 5, 3427−3433

temperatures can come from "superheating" effects that can elevate the transition temperatures by up to 100 K[35] and that a similar overestimation was calculated for $PC_{61}BM$.[28,30] Taking into consideration the 85:15 α/β blend, the simulated melting temperature reduces by ∼20 K, which indicates that the intermolecular interactions among the fullerenes in the isomeric mixture are not as strong as those in the pure material; in other words, the presence of isomers disrupts the molecular packing to some extent. The experimentally observed melting point of amorphous $PC_{61}BM$ is 557 K,[38,39] some 35 K less than $PC_{71}BM$, a trend that is reproduced by the simulations (630 K for $PC_{61}BM$).

Interestingly, the simulations for the pure $PC_{71}BM$ α-isomer reveal an increase in density at approximately 450 K, a feature that has been experimentally reported at 477 K as a cold-crystallization event.[37] The density increase can be attributed to the fact that the thermal energy provided to the $PC_{71}BM$ molecules leads to molecular reorientation (rotational and translational motion), and these reorientations allow the packing to steer away from the jammed state toward the global equilibrium. The voids in the jammed packing are filled upon reorientation (i.e., increasing the kinetic energy of the molecules is akin to the shaking of jars to fill more beads), resulting in the density increase. Jammed packings of ellipsoids are observed as a function of ellipsoid concentration and temperature.[40] Because rotational and translational degrees of freedom are lost at different temperatures or packing fractions (for granular solids, the packing fraction is defined as the amount of space filled by the material, for example, the packing fraction of spheres in a face-centered cubic fcc structure is ∼0.74), multiple phase transitions can be observed in ellipsoidal packings;[41,42] the simulations here reveal similar events for $PC_{71}BM$.

The liquid-crystal order parameter (S; see the SI for the definition) can also be used to evaluate the presence of order−disorder transitions as a function of temperature. While the liquid-crystal order parameter is not particularly useful to observe thermal transitions in amorphous systems, the sudden spike in the degree of order at 450 K in the $PC_{71}BM$ systems corresponds to the same temperature range as the increased density arising in the density versus temperature plot, supporting the assignment of a phase transition. In the order parameter plot for $PC_{61}BM$ and the 85:15 regioisomer blend of $PC_{71}BM$, no distinct jumps in density (of similar magnitude as that observed for the $PC_{71}BM$ α-isomer) are observed, indicating that the change in molecular packing (top panel of Figure 2) and density increase (bottom panel of Figure 2) do not occur in these systems with increasing temperature.

We note that negative values for the order parameters indicate slight ordering, while order parameters of 0.02−0.05 (due to finite size effects) imply disordered/isotropic packing.[27] These results suggest that the barrier for reorientation (e.g., the necessary degrees of freedom in ellipsoids relative to spheres to allow for reorientation) is approximately 4 kJ/mol (1 kcal/mol), corresponding to a temperature range of 450−500 K, such that the energy conferred to the system in this temperature range is enough to allow for a partially ordered $PC_{71}BM$ to become isotropically ordered.

To relate such changes in orientation to temperature, plots of the orientation distribution function (ODF) as a function of temperature are given in Figure S1 in the SI. The orientation is computed between the vectors defined by a straight line connecting the center-of-mass (COM) of the fullerene cage to the methano-bridge carbon linked to the cage. Below 500 K, the $PC_{71}BM$ ODFs for the α-isomer and the isomer blend have two symmetric peaks at 65 and 115°, indicating that the $PC_{71}BM$ molecules have a preferential orientation; this result is similar to the invariant observed for deposited prolate ellipsoids with aspect ratios of 1.6.[43] On the other hand, the ODF for $PC_{61}BM$ reveals a single peak at 90°, a feature that is also indicative of ellipsoidal packing; as noted above, functionalization of (perfectly) spherical C_{60} molecules renders the substituted fullerene as an ellipsoid (aspect ratio of 1.19 if the methano-bridge carbon atom is taken into account). Viewing $PC_{71}BM$ through the same lens (now with an axial aspect ratio of 1.33) suggests that if the $PC_{71}BM$ molecules were perfect ellipsoids, they should pack densely with significant long-range order;[27,40,41,43−45] however, the presence of the phenyl−butyric acid−methyl ester group renders $PC_{71}BM$ an imperfect ellipsoid with reduced packing ability.

Radial distribution functions (RDFs) for substituted fullerenes at 300 K are given in Figure 3. As the RDF represents

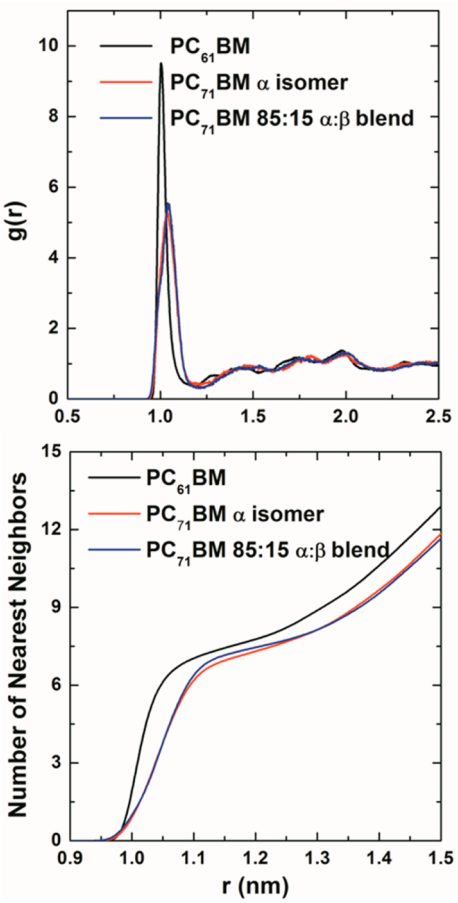

Figure 3. (Top) Fullerene−fullerene COM RDFs $g(r)$ (RDFs) for $PC_{61}BM$ and $PC_{71}BM$ and (bottom) number of nearest neighbors as a function of distance for amorphous $PC_{61}BM$ and the $PC_{71}BM$ α-isomer and isomeric blend.

the local packing density in comparison to the average molecular density, the sharper first peak for $PC_{61}BM$ as compared to that for $PC_{71}BMs$ indicates that the $PC_{61}BM$ molecules have a more consistent distance with their first-shell neighbors; the broader peak for the $PC_{71}BMs$ is due to a greater variation in distance of the first-shell neighbors, a function of the larger volume and asymmetry of the axial

dx.doi.org/10.1021/jz501559q | J. Phys. Chem. Lett. 2014, 5, 3427−3433

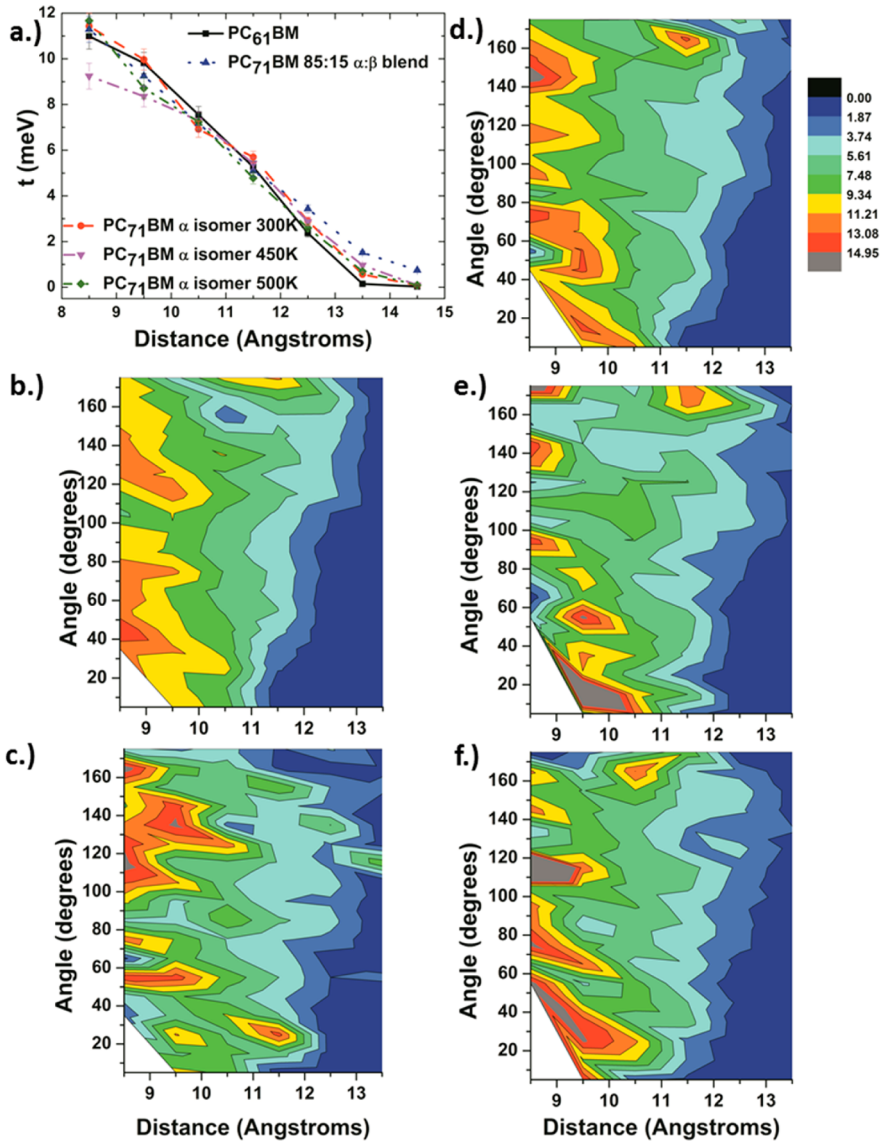

Figure 4. (a) Average LUMO−LUMO electronic couplings t (meV) as a function of distance for $PC_{61}BM$ and $PC_{71}BM$. Note that consideration of the adduct in the COM calculations allows for the distance to be less than 0.9 nm between two $PC_{71}BM$ molecules, especially at angles greater than 20°. Error bars are the standard deviation from three independent calculations. Contour plots of the electronic couplings as a function of distance and angle for (b) $PC_{61}BM$ at 300 K, (c) the 85:15 α/β $PC_{71}BM$ blend at 300 K, (d) the $PC_{71}BM$ α-isomer at 300 K, (e) the $PC_{71}BM$ α-isomer at 450 K, and (f) the $PC_{71}BM$ α-isomer at 500 K.

lengths of the ellipsoidal $PC_{71}BM$ fullerene. The RDFs for both the pure α-isomer material and the α/β blend do not differ significantly beyond the first shell. The number of nearest neighbors in the first shell is 7.7 (integrating up to the first valley in the $PC_{61}BM$ RDF, i.e., 1.20 nm) for $PC_{61}BM$, whereas it is 8.14 (1.3 nm) for $PC_{71}BM$. These values agree well with reported work regarding the positive relationship between the number of neighbors and aspect ratios below a critical aspect ratio (2.0).[44] The number of nearest neighbors in the isomeric blend is almost equal to that in the pure α-isomer, though minor orientational differences are noted and can be interpreted as a contribution to polydispersity in the packed ellipsoids (because in the isomeric blend, the $PC_{71}BM$ molecules can be viewed as ellipsoids with different axis dimensions, thereby creating a polydisperse mix). The decreased order parameter for polydisperse prolate ellipsoids at similar aspect ratios suggests that having isomeric blends of $PC_{71}BM$ in thin films will introduce disordered regions within ordered domains.[43]

Thus, far, we have noted how variations in fullerene shape introduce changes in the thermal transition temperatures and packing configurations. The structural differences for $PC_{71}BM$ suggest that the effects of the fullerene asymmetry and molecule size alter molecular packing and order. Recent work from our group highlighted how differences in molecular size (disks of varied sizes) in blend materials can affect material miscibility.[46] In addition, studies on molecular shape indicate that increasing the size of spheres (in mixtures of disks and spheres) influences miscibility.[47] As such, the larger size and ellipsoid shape of $PC_{71}BM$ can positively influence miscibility/crystallinity with many commonly used rigid donor polymers as compared to the more spherical $PC_{61}BM$. The impact of this attribute can be seen in the comparison of OSC active layers derived from $PC_{71}BM$/poly[*N*-900-hepta-decanyl-2,7-carbazole-*alt*-5,5-(40,70-di-2-thienyl-20,10,30-benzothiadiazole)][48]

dx.doi.org/10.1021/jz501559q | J. Phys. Chem. Lett. 2014, 5, 3427−3433

(PCDTBT) with respect to $PC_{61}BM$/PCDTBT;[49] in the former, near 100% quantum efficiencies are observed, which is due to improved film morphology (along with broader photoabsorption). Importantly, the optimized processing procedures for these two films differed, even though they both used the same polymer with a substituted fullerene; this is a direct result of the differences noted above in terms of phase transitions due to the variations in molecular shape and packing. Similar studies on fullerene/poly(3-hexylthiophene) films also reveal differences in material miscibility and the resulting film morphology (under identical processing procedures) as a function of the nature of the substituted fullerene.[50,51]

We now turn to an assessment of how the molecular-shape-induced packing differences influence intermolecular electronic couplings (transfer integrals). The ability to readily delocalize charges and assist in the efficient dissociation of excitons is one of the key elements among the electronic processes taking place in OSCs;[31,32] in such a context, the extent of electronic communication among adjacent fullerene molecules can thus play a major role. In order to connect the structural properties with this key characteristic, we have evaluated the intermolecular electronic couplings between the LUMO wave functions of adjacent $PC_{71}BM$ dimers within the first-neighbor shell. As can be seen from Figure 4, the *average* electronic couplings are similar for $PC_{71}BM$ and $PC_{61}BM$, with $PC_{71}BM$ exhibiting very slightly larger electronic couplings. Hence, the minor differences seen in molecular packing lead to nearly no difference in these average intermolecular electronic couplings. However, at temperatures greater than the cold crystallization temperature (here 500 K), there is a notable increase in electronic couplings for $PC_{71}BM$ (diamonds in Figure 4a). These results underline how annealing $PC_{71}BM$ at temperatures close to the cold crystallization temperature can affect the electronic couplings, and ultimately the electronic processes, within $PC_{71}BM$ domains and potentially at donor−acceptor interfaces.

Contour plots of the intermolecular electronic couplings as a function of orientation and distance for molecules in the first-neighbor shell are also shown in Figure 4. $PC_{61}BM$ and $PC_{71}BM$ overall display similar orientation−electronic coupling behaviors. However, some important distinctions can be pointed out. $PC_{61}BM$ shows broad peaks with fairly large (relative) electronic couplings from 30 to 75° and 120 to 150°. In $PC_{71}BM$, on the other hand, there are multiple specific angles at which the electronic couplings are large. These distinctive peaks directly arise from the more ellipsoidal shape of the fullerene in $PC_{71}BM$. In addition, both the spatial and wave function overlaps of neighboring five-membered or six-membered rings maximize at more orientations in ellipsoidal structures as compared to spheres. These trends continue at high temperatures, with the peaks becoming sharper and more distinct with increasing temperature, for example, the peak at 12.0 Å and 165° at 300 K as compared to the peak at 11.0 Å and 165° at 500 K. There is also a trend toward stronger electronic couplings for the higher-temperature structures, indicative of the positive effects described above. For the α/β blends, the trends at 300 K are similar to those of the α-isomer, though the introduction of a new peak at 11.0−12.0 Å and 30° reveals how the orientational differences induced by the regioisomers impact the electronic couplings.

To summarize, in this work we have used MD simulations coupled with electronic structure calculations to examine how the ellipsoidal shape of $PC_{71}BM$ imparts differences in the materials' packing and properties compared to $PC_{61}BM$. The main conclusions we can draw are as follows:

- $PC_{71}BM$ should have similar compatibility with solvents and other molecular materials as $PC_{61}BM$. However, increased miscibilities with $PC_{71}BM$ can arise due to the increased volume and surface area of the ellipsoidal shape.
- Within the first shell of neighboring molecules, the elliptical (less symmetric) shape of $PC_{71}BM$ makes the nearest neighbors appear at somewhat different distances compared to the nearly equal distances in $PC_{61}BM$; the number of first-shell neighbors is also slightly higher for $PC_{71}BM$. The preferential orientations of $PC_{71}BM$ molecules when compared to $PC_{61}BM$ point to the ability of $PC_{71}BM$ molecules to pack with larger degrees of crystallinity.
- Minor structural differences in the packing of the pure α-isomer versus the isomeric blend of $PC_{71}BM$ change the onset of loss of either translational or rotational degrees of freedom, resulting in modified transition temperatures. This result is important when comparing $PC_{61}BM$ and $PC_{71}BM$ as it indicates that the annealing temperatures required to alter the morphology of BHJ-active layers should differ as a function of the fullerene employed.
- Variations in molecular packing lead to notable differences in the evolution of the electronic couplings as a function of orientation. As such, the resulting electronic properties of fullerene aggregates (e.g., state energies, degrees of charge localization/delocalization) can significantly differ. Quantifying these aspects will be the focus of future studies.

Overall, our results emphasize that care needs to be taken when evaluating the intrinsic electronic processes in fullerene-based materials because the packing differences among the fullerenes have to be appropriately taken into account. These packing differences must also be considered when modeling the processes of photocurrent generation in OSCs based on fullerene derivatives.

■ ASSOCIATED CONTENT

Ⓢ Supporting Information

Computational methodology, Hildebrand and Hansen solubility parameters, definitions for the liquid-crystal order parameter, and orientational distribution functions (ODFs) for the systems discussed. This material is available free of charge via the Internet at http://pubs.acs.org.

■ AUTHOR INFORMATION

Corresponding Authors

*E-mail: chad.risko@uky.edu (C.R.).
*E-mail: jean-luc.bredas@kaust.edu.sa (J.-L.B.).

Present Addresses

[#]M.W.: Kings College, 133 North River Street, Wilkes-Barre, PA 18711, United States.
[§]C.R.: Department of Chemistry and Center for Applied Energy Research (CAER), University of Kentucky, Lexington, Kentucky 40506-0055, United States.
[⊥]J.L.B.: Division of Physical Sciences and Engineering, King Abdullah University of Science and Technology − KAUST, Thuwal 23955-6900, Kingdom of Saudi Arabia.

Notes

The authors declare no competing financial interest.

■ ACKNOWLEDGMENTS

We gratefully acknowledge the support of various parts of this work by the Deanship of Scientific Research of King Abdulaziz University under an International Collaboration Grant (Award No. D-001-433), the Office of Naval Research (Award No. N00014141-0171), and the National Science Foundation through the Hooked on Photonics Research Experience for Undergraduates (REU) Program (Award No. CHE-1156598).

■ REFERENCES

(1) Morel, D. L.; Ghosh, A. K.; Feng, T.; Stogryn, E. L.; Purwin, P. E.; Shaw, R. F.; Fishman, C. High-Efficiency Organic Solar Cells. *Appl. Phys. Lett.* **1978**, *32*, 495−497.

(2) Tang, C. W. Two-Layer Organic Photovoltaic Cell. *Appl. Phys. Lett.* **1986**, *48*, 183−185.

(3) Hiramoto, M.; Fujiwara, H.; Yokoyama, M. Three-Layered Organic Solar Cell with a Photoactive Interlayer of Codeposited Pigments. *Appl. Phys. Lett.* **1991**, *58*, 1062−1064.

(4) Halls, J. J. M.; Walsh, C. A.; Greenham, N. C.; Marseglia, E. A.; Friend, R. H.; Moratti, S. C.; Holmes, A. B. Efficient Photodiodes from Interpenetrating Polymer Networks. *Nature* **1995**, *376*, 498−500.

(5) Yu, G.; Gao, J.; Hummelen, J. C.; Wudl, F.; Heeger, A. J. Polymer Photovoltaic Cells — Enhanced Efficiencies Via a Network of Internal Donor−Acceptor Heterojunctions. *Science* **1995**, *270*, 1789−1791.

(6) Risko, C.; McGehee, M. D.; Bredas, J. L. A Quantum-Chemical Perspective into Low Optical-Gap Polymers for Highly-Efficient Organic Solar Cells. *Chem. Sci.* **2011**, *2*, 1200−1218.

(7) Potscavage, W. J.; Sharma, A.; Kippelen, B. Critical Interfaces in Organic Solar Cells and Their Influence on the Open-Circuit Voltage. *Acc. Chem. Res.* **2009**, *42*, 1758−1767.

(8) Anthony, J. E.; Facchetti, A.; Heeney, M.; Marder, S. R.; Zhan, X. n-Type Organic Semiconductors in Organic Electronics. *Adv. Mater.* **2010**, *22*, 3876−3892.

(9) Kippelen, B.; Bredas, J. L. Organic Photovoltaics. *Energy Environ. Sci.* **2009**, *2*, 251−261.

(10) Bredas, J. L.; Norton, J. E.; Cornil, J.; Coropceanu, V. Molecular Understanding of Organic Solar Cells: The Challenges. *Acc. Chem. Res.* **2009**, *42*, 1691−1699.

(11) Hoppe, H.; Sariciftci, N. S. Organic Solar Cells: An Overview. *J. Mater. Res.* **2004**, *19*, 1924−1945.

(12) Thompson, B. C.; Fréchet, J. M. J. Polymer−Fullerene Composite Solar Cells. *Angew. Chem., Int. Ed.* **2008**, *47*, 58−77.

(13) You, J. B.; Dou, L. T.; Yoshimura, K.; Kato, T.; Ohya, K.; Moriarty, T.; Emery, K.; Chen, C. C.; Gao, J.; Li, G.; et al. A Polymer Tandem Solar Cell with 10.6% Power Conversion Efficiency. *Nat. Commun.* **2013**, *4*, 1446.

(14) Liu, Y.; Chen, C.-C.; Hong, Z.; Gao, J.; Yang, Y.; Zhou, H.; Dou, L.; Li, G.; Yang, Y. Solution-Processed Small-Molecule Solar Cells: Breaking the 10% Power Conversion Efficiency. *Sci. Rep.* **2013**, *3*, 3356.

(15) Wienk, M. M.; Kroon, J. M.; Verhees, W. J. H.; Knol, J.; Hummelen, J. C.; van Hal, P. A.; Janssen, R. A. J. Efficient Methano[70]Fullerene/MDMO-PPV Bulk Heterojunction Photovoltaic Cells. *Angew. Chem., Int. Ed.* **2003**, *42*, 3371−3375.

(16) Hummelen, J. C.; Knight, B. W.; LePeq, F.; Wudl, F.; Yao, J.; Wilkins, C. L. Preparation and Characterization of Fulleroid and Methanofullerene Derivatives. *J. Org. Chem.* **1995**, *60*, 532−538.

(17) Vakhshouri, K.; Kozub, D. R.; Wang, C. C.; Salleo, A.; Gomez, E. D. Effect of Miscibility and Percolation on Electron Transport in Amorphous Poly(3-hexylthiophene)/Phenyl-C_{61}-Butyric Acid Methyl Ester Blends. *Phys. Rev. Lett.* **2012**, *108*, 026601.

(18) Bloking, J. T.; Han, X.; Higgs, A. T.; Kastrop, J. P.; Pandey, L.; Norton, J. E.; Risko, C.; Chen, C. E.; Bredas, J. L.; McGehee, M. D.; et al. Solution-Processed Organic Solar Cells with Power Conversion Efficiencies of 2.5% Using Benzothiadiazole/Imide-Based Acceptors. *Chem. Mater.* **2011**, *23*, 5484−5490.

(19) Zhang, X.; Lu, Z.; Ye, L.; Zhan, C.; Hou, J.; Zhang, S.; Jiang, B.; Zhao, Y.; Huang, J.; Zhang, S.; et al. A Potential Perylene Diimide Dimer-Based Acceptor Material for Highly Efficient Solution-Processed Non-Fullerene Organic Solar Cells with 4.03% Efficiency. *Adv. Mater.* **2013**, *25*, 5791−5797.

(20) Zang, Y.; Li, C.-Z.; Chueh, C.-C.; Williams, S. T.; Jiang, W.; Wang, Z.-H.; Yu, J.-S.; Jen, A. K. Y. Integrated Molecular, Interfacial, and Device Engineering Towards High-Performance Non-Fullerene Based Organic Solar Cells. *Adv. Mater.* **2014**, *26*, 5708−5714.

(21) Cnops, K.; Rand, B. P.; Cheyns, D.; Verreet, B.; Empl, M. A.; Heremans, P. 8.4% Efficient Fullerene-Free Organic Solar Cells Exploiting Long-Range Exciton Energy Transfer. *Nat. Commun.* **2014**, *5*, 3406.

(22) Hou, J.; Guo, X. Active Layer Materials for Organic Solar Cells. In *Organic Solar Cells: Materials and Device Physics*; Choy, W. C. H., Ed.; Springer-Verlag: London, 2013; pp 17−42.

(23) Morvillo, P. Higher Fullerenes as Electron Acceptors for Polymer Solar Cells: A Quantum Chemical Study. *Sol. Energy Mater. Sol. Cells* **2009**, *93*, 1827−1832.

(24) Meng, X.; Zhao, G.; Xu, Q.; Tan, Z.; Zhang, Z.; Jiang, L.; Shu, C.; Wang, C.; Li, Y. Effects of Fullerene Bisadduct Regioisomers on Photovoltaic Performance. *Adv. Funct. Mater.* **2014**, *24*, 158−163.

(25) Matsuo, Y.; Kawai, J.; Inada, H.; Nakagawa, T.; Ota, H.; Otsubo, S.; Nakamura, E. Addition of Dihydromethano Group to Fullerenes to Improve the Performance of Bulk Heterojunction Organic Solar Cells. *Adv. Mater.* **2013**, *25*, 6266−6269.

(26) Wong, W. W. H.; Subbiah, J.; White, J. M.; Seyler, H.; Zhang, B.; Jones, D. J.; Holmes, A. B. Single Isomer of Indene-C_{70} Bisadduct—Isolation and Performance in Bulk Heterojunction Solar Cells. *Chem. Mater.* **2014**, *26*, 1686−1689.

(27) Donev, A.; Cisse, I.; Sachs, D.; Variano, E. A.; Stillinger, F. H.; Connelly, R.; Torquato, S.; Chaikin, P. M. Improving the Density of Jammed Disordered Packings Using Ellipsoids. *Science* **2004**, *303*, 990−993.

(28) Tummala, N. R.; Mehraeen, S.; Fu, Y.-T.; Risko, C.; Bredas, J. L. Materials-Scale Implications of Solvent and Temperature on [6,6]-Phenyl-C_{61}-Butyric Acid Methyl Ester (PCBM): A Theoretical Perspective. *Adv. Funct. Mater.* **2013**, *23*, 5800−5813.

(29) Cheung, D. L.; Troisi, A. Theoretical Study of the Organic Photovoltaic Electron Acceptor PCBM: Morphology, Electronic Structure, and Charge Localization. *J. Phys. Chem. C* **2010**, *114*, 20479−20488.

(30) Frigerio, F.; Casalegno, M.; Carbonera, C.; Nicolini, T.; Meille, S. V.; Raos, G. Molecular Dynamics Simulations of the Solvent- and Thermal History-Dependent Structure of the Pcbm Fullerene Derivative. *J. Mater. Chem.* **2012**, *22*, 5434−5443.

(31) Gélinas, S.; Rao, A.; Kumar, A.; Smith, S. L.; Chin, A. W.; Clark, J.; van der Poll, T. S.; Bazan, G. C.; Friend, R. H. Ultrafast Long-Range Charge Separation in Organic Semiconductor Photovoltaic Diodes. *Science* **2014**, *343*, 512−516.

(32) Savoie, B. M.; Rao, A.; Bakulin, A. A.; Gelinas, S.; Movaghar, B.; Friend, R. H.; Marks, T. J.; Ratner, M. A. Unequal Partnership: Asymmetric Roles of Polymeric Donor and Fullerene Acceptor in Generating Free Charge. *J. Am. Chem. Soc.* **2014**, *136*, 2876−2884.

(33) Hildebrand, J. H.; Scott, R. L. The Entropy of Solution of Nonelectrolytes. *J. Chem. Phys.* **1952**, *20*, 1520−1521.

(34) Hansen, C. M. "The Three Dimensional Solubility Parameter-Key to Paint Component Affnitiies": I. Solvents, Plasticizers, Polymers and Resins. *J. Paint Technol.* **1967**, *39*, 104.

(35) Watt, S. W.; Chisholm, J. A.; Jones, W.; Motherwell, S. A Molecular Dynamics Simulation of the Melting Points and Glass Transition Temperatures of Myo- and Neo-Inositol. *J. Chem. Phys.* **2004**, *121*, 9565−9573.

(36) Soldera, A. Comparison between the Glass Transition Temperatures of the Two PMMA Tacticities: A Molecular Dynamics Simulation Point of View. *Macromol. Symp.* **1998**, *133*, 21−32.

(37) Miller, N. C.; Gysel, R.; Miller, C. E.; Verploegen, E.; Beiley, Z.; Heeney, M.; McCulloch, I.; Bao, Z.; Toney, M. F.; McGehee, M. D. The Phase Behavior of a Polymer−Fullerene Bulk Heterojunction System That Contains Bimolecular Crystals. *J. Polym. Sci., Part B: Polym. Phys.* **2011**, *49*, 499−503.

(38) Zheng, L.; Han, Y. Solvated Crystals Based on [6,6]-Phenyl-C_{61}-butyric Acid Methyl Ester (PCBM) with the Hexagonal Structure and Their Phase Transformation. *J. Phys. Chem. B* **2012**, *116*, 1598−1604.
(39) Jamieson, F. C.; Domingo, E. B.; McCarthy-Ward, T.; Heeney, M.; Stingelin, N.; Durrant, J. R. Fullerene Crystallisation as a Key Driver of Charge Separation in Polymer/Fullerene Bulk Heterojunction Solar Cells. *Chem. Sci.* **2012**, *3*, 485−492.
(40) Donev, A.; Stillinger, F. H.; Chaikin, P. M.; Torquato, S. Unusually Dense Crystal Packings of Ellipsoids. *Phys. Rev. Lett.* **2004**, *92*, 255506.
(41) Zheng, Z.; Wang, F.; Han, Y. Glass Transitions in Quasi-Two-Dimensional Suspensions of Colloidal Ellipsoids. *Phys. Rev. Lett.* **2011**, *107*, 065702.
(42) Mishra, C. K.; Rangarajan, A.; Ganapathy, R. Two-Step Glass Transition Induced by Attractive Interactions in Quasi-Two-Dimensional Suspensions of Ellipsoidal Particles. *Phys. Rev. Lett.* **2013**, *110*, 188301.
(43) Baram, R. M.; Lind, P. G. Deposition of General Ellipsoidal Particles. *Phys. Rev. E* **2012**, *85*, 041301.
(44) Buchalter, B. J.; Bradley, R. M. Orientational Order in Amorphous Packings of Ellipsoids. *Europhys. Lett.* **1994**, *26*, 159.
(45) Dorosz, S.; Schilling, T. Crystallization in Glassy Suspensions of Hard Ellipsoids. *J. Chem. Phys.* **2013**, *139*, 124508.
(46) Wunsch, B. H.; Rumi, M.; Tummala, N. R.; Risko, C.; Kang, D.-Y.; Steirer, K. X.; Gantz, J.; Said, M.; Armstrong, N. R.; Bredas, J. L.; et al. Structure-Processing-Property Correlations in Solution-Processed, Small-Molecule, Organic Solar Cells. *J. Mater. Chem. C* **2013**, *1*, 5250−5260.
(47) Oversteegen, S. M.; Lekkerkerker, H. N. W. Phase Diagram of Mixtures of Hard Colloidal Spheres and Discs: A Free-Volume Scaled-Particle Approach. *J. Chem. Phys.* **2004**, *120*, 2470−2474.
(48) Park, S. H.; Roy, A.; Beaupre, S.; Cho, S.; Coates, N.; Moon, J. S.; Moses, D.; Leclerc, M.; Lee, K.; Heeger, A. J. Bulk Heterojunction Solar Cells with Internal Quantum Efficiency Approaching 100%. *Nat. Photonics* **2009**, *3*, 297−302.
(49) Wakim, S.; Beaupre, S.; Blouin, N.; Aich, B.-R.; Rodman, S.; Gaudiana, R.; Tao, Y.; Leclerc, M. Highly Efficient Organic Solar Cells Based on a Poly(2,7-carbazole) Derivative. *J. Mater. Chem.* **2009**, *19*, 5351−5358.
(50) Chen, H. P.; Peet, J.; Hsiao, Y. C.; Hu, B.; Dadmun, M. The Impact of Fullerene Structure on Its Miscibility with P3HT and Its Correlation of Performance in Organic Photovoltaics. *Chem. Mater.* **2014**, *26*, 3993−4003.
(51) Collins, B. A.; Tumbleston, J. R.; Ade, H. Miscibility, Crystallinity, and Phase Development in P3HT/PCBM Solar Cells: Toward an Enlightened Understanding of Device Morphology and Stability. *J. Phys. Chem. Lett.* **2011**, *2*, 3135−3145.